Investigation on the Micromechanisms of the Cracking of 316L Heat Exchanger Tubes

Hui XU[1], Lulu FANG, Qiaofeng DING, Yanjun GUO, Xiaohui LI, Lu WANG and Lin YANG

Department of Materials Technology, Huadian Electric Power Research Institute Co., Ltd., Hangzhou, China

Abstract. The cracking mechanisms of 316L heat exchanger tubes employed in power station were studied using optical microscope (OM) and scanning electron microscope (SEM). It is demonstrated that the hardness value, microstructure and tensile properties of selected #1 and #2 tube samples all meet the requirements of relevant standards, but the contents of Ni and Mo element of #1 tube are slightly lower than the standard requirements. The circumferential cracks on the two samples nucleate at the corrosion pits on the inner wall of the tubes, while Cl element was detected in the corrosion products of these pits. The cracks propagate from the inner wall to the outer wall along the circumferential direction of the tube, forming a dendritic crack morphology with both transgranular and intergranular propagation characteristics. Combined with the investigation of the service condition of the heat exchanger tubes and the analysis of the experimental results, it can be concluded that the main reason for cracking is the initiation of pin-corrosion when the content of chloride ion exceeds the standard during the service of the tubes, which will induce stress corrosion cracking, causing crack expansion through the wall thickness, and finally lead to leakage of the tube. In addition, from the point of view of materials, Mo is an important element to improve the pitting resistance of materials. The content of Mo element detected in the samples is lower than the standard requirement, which is also one of the reasons for the easy pitting corrosion of the inner wall of the pipe.

Keywords. Heat exchanger tubes, power station, pin-corrosion

1. Introduction

316L is a kind of ultra-low carbon austenitic stainless steel containing Mo element, with excellent corrosion resistance, good mechanical properties and welding properties [1]. 316L stainless steel is widely used, and the common corrosion modes include intergranular corrosion, stress corrosion cracking, crevice corrosion, naphthenic acid corrosion, atmospheric corrosion and seawater corrosion. High temperature, high Cl^{-1} content, residual stress, stress concentration can jointly promote stress corrosion cracking [2-4]. Stress corrosion cracking is caused by the combined action of stress corrosion sensitivity of materials, corrosive media, stress and other factors [5-7]. The critical Cl^{-1} concentration that leading to stress corrosion cracking is affected by

[1] Corresponding Author, Hui XU, Department of Materials Technology, Huadian Electric Power Research Institute Co., Ltd., Hangzhou, China; Email: 125894620@qq.com.

various factors such as water quality, temperature, flow rate, water stabilizer and so on [8]. The heat network heaters of thermal power plants are usually designed as tubes in the materials of 304 and 316L, etc. Once the water quality is not up to standard in the service process, corrosion and scaling will occur at best, affecting the heat transfer efficiency; at worst, perforation will occur, resulting in interruption of heating supply and huge economic losses [9, 10].

Obvious leakage was detected at the upper tube bundle of a heater, leading to the leakage of water to both sides of the heater employed in the heat-network heaters in a power plant. In order to find the underlying reason for the leakage, systematic experiments were carried out in order to check the material properties of the tube. The heat exchanger tubes were made of 316L stainless steel with the dimensions of 19mm in diameter and a thickness of 1mm. The total running time of the tubes were about 7500 hours, with steam side temperature (outside the bundle) is 395°C, the steam pressure is 0.35MPa, the water side (inside the bundle) temperature is 70-130°C, the water side pressure is 2.1MPa.

2. Experimental Materials and Methods

Two cracked heat exchanger tubes were selected as experimental samples in this paper, which are recorded as #1 and #2 samples respectively. Systematic tests on the chemical composition, Vickers hardness, metallographic microstructures, tensile properties, crack morphology, corrosion products were carried out in the two samples in order find out the leakage reason. The specimens of chemical composition were prepared by cutting the clamping end of tensile specimen. Vickers hardness and metallographic microstructure inspection were conducted on the same specimen machined near the cracking area. Tensile tests were carried out at room temperature, two specimens were tested for each tube, which is cut at about 50 mm away from the cracking area. The observation of crack morphology shares the same specimen to the inspection of corrosion products in both tube samples, using an optical microscope (OM) and a scanning electron microscope (SEM), respectively.

The appearance of the cracked heat exchange tubes is shown in figure 1. There is a penetrating torodirectional crack (indicated by the arrow in the figure) with a length of 5-8mm in each cracked tube. However, there is no obvious mechanical damage around the crack, also without any obvious swelling, wall thickness thinning or plastic deformation.

Figure 1. Macroscopic appearance of two tube samples.

3. Results

3.1. Spectrum Inspection

The ARL8860 direct-reading spectrometer was used to determine the composition of the #1 tube. The results are shown in table 1. It can be seen that the contents of Ni and Mo in the tube are slightly lower than the requirements of ASTM A213/ A213M-19A standard, and the contents of other elements meet the requirements of the standard. From the point of view of materials, Mo is an important element to improve the pitting resistance of materials. The content of Mo element detected in the sample is lower than the standard requirement, which is one of the reasons for the poor pitting resistance of the inner wall of the tube.

Table 1. The chemical compositions of #1 tube (Wt. %).

Specimen	C	Mn	P	S	Si	Cr	Ni	Mo
standard values	≤0.035	≤2.00	≤0.045	0.030	1.00	16.0-18.0	10.0-14.0	2.00-3.00
#1 tube	0.009	1.45	0.026	0.000	0.55	16.3	8.8	1.81

3.2. Mechanical Property Tests

Vickers hardness tester was used to examine the hardness of tube sample, and 6 points are randomly selected and measured for each tube. As shown in table 2, the average value of Vickers hardness in #1 tube is 156, which is near to the Vickers hardness in #2 tube. Moreover, the Vickers hardness of #1 and #2 tube all meet the requirements of ASTM A213/ A213M-19a standard as listed in table 2. The tensile results of two tube samples were depicted in table 3. The yield strength, tensile strength and elongation in each tube have little difference, and all meet the requirements of ASTM A213/ A213M-19a standard.

Table 2. The Vickers hardness of two specimens (HV).

Specimens	1	2	3	4	5	6	Average value	Standard value
#1	146	148	158	160	162	164	156	≤200
#2	136	145	147	149	149	154	147	

Table 3. Tensile properties of tested specimens.

Specimen	Yield strength MPa	Tensile strength (MPa)	Elongation (%)
#1-1	298	661	54.5
#1-2	262	655	56.0
#2-1	273	663	53.0
#2-2	270	671	55.0
Standard value	≥170	≥485	≥35.0

3.3. Metallographic Observation

The microstructures of tube samples of #1 and #2 are shown in figure 2. It can be found that both tubes have the austenitic structure with a few annealing twins in some grains

and coarse granular carbides imbedded along grain boundaries. There is no significant difference in microstructures between the two tubes, and the aging grade of two tubes is about 2.5.
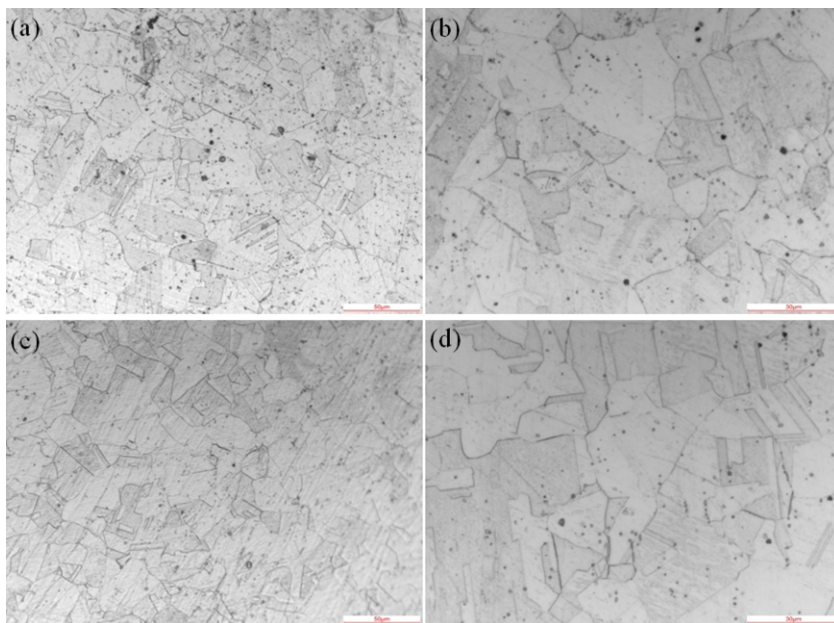

Figure 2. OM inspection of microstructures in two tubes: (a) #1, 500×; (b) #1, 1000×; (c) #2, 500×; (d) #2, 1000×.

3.4. Crack Morphology

The morphology of crack propagation on the outer surface of #2 tube was depicted in figure 3. It can be seen that there are several small secondary cracks near the toroidal main crack surface, and the secondary cracks will further bifurcate in the process of propagation, forming dendritic crack propagation morphology (figure 3a). The magnified picture of multiple branching cracks reveal that the propagation mode of these cracks was dominated by both intergranular and transgranular characteristics. The microcracks and the main cracks connect with each other, and then propagated toward the outer wall of the tube (figures 3b and 3c).

The cracking morphology at inner wall of #1 tube was shown in figure 4. It can be found that the crack width in the middle of a pitting corrosion pit on the inner wall of the tube is the largest, while the crack width that keeping away from the middle position of the pit gradually decreases. It can be deduced that it was the position of cracking source. Further observation demonstrates that one end of the crack propagated along the ring towards the outer wall of the tube, and finally penetrated into the outer surface of the sample. While the other end of the crack propagated more slowly, the crack tip locates near the corrosion pit. The crack nucleation area is covered with a thick layer of corrosion products, which are gray-white, smooth surface, sharp edges and corners, and many micro-cracks are formed due to its crushing.
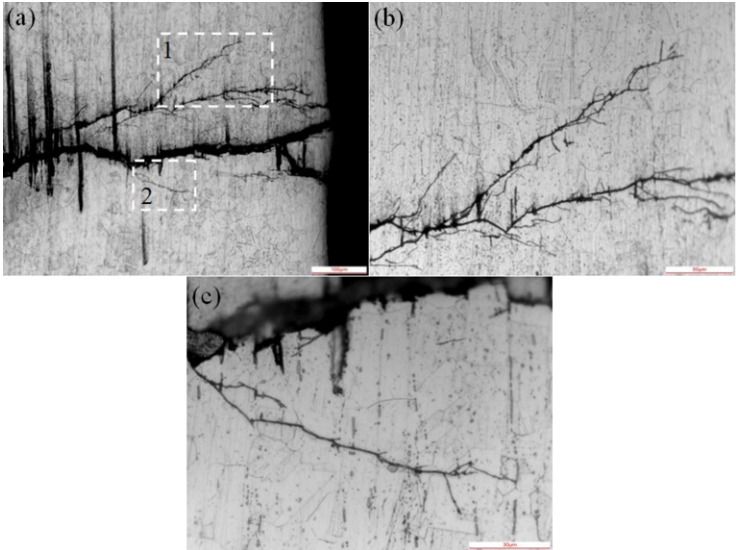
Figure 3. Crack morphology of #2 tube: (a) overall look; (b) partial enlarged view of block 1; (c) partial enlarged view of block 2.
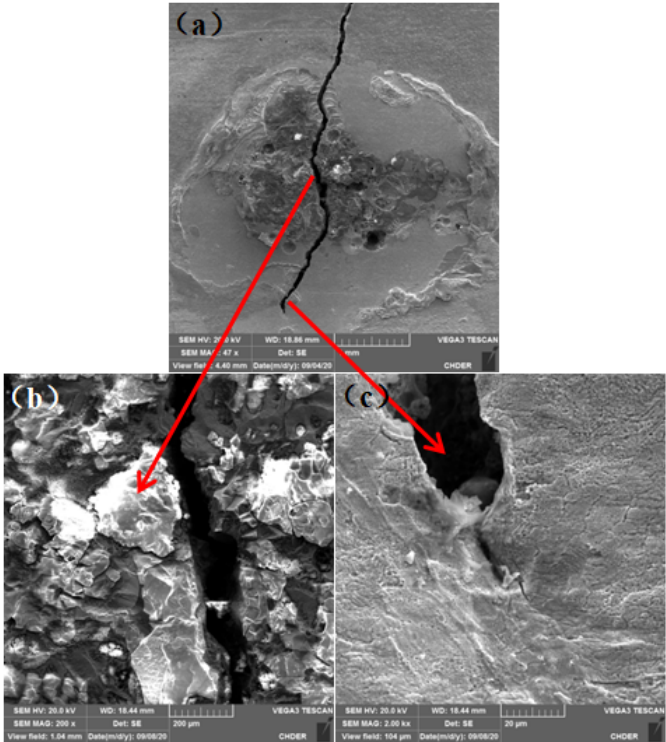

Figure 4. Crack morphology on the inner wall of #1 tube: (a) corrosion pit; (b) nucleation site; (c) crack tip.

Further observation found that there were smaller size of corrosion products and corrosion pits in the local area of the inner wall of the two tubes. As shown in figures

5a and 5b, small-size corrosion pits in #1, #2 tubes are produced by the exfoliating of corrosion products with a certain number of spherical inclusions. The continuous formation and shedding of corrosion products also resulted in the formation of small cataphracted corrosion pits in local areas, and these small corrosion pits would gradually converge and merge into larger corrosion pits, finally generating cracks (figures 5c and 5d).
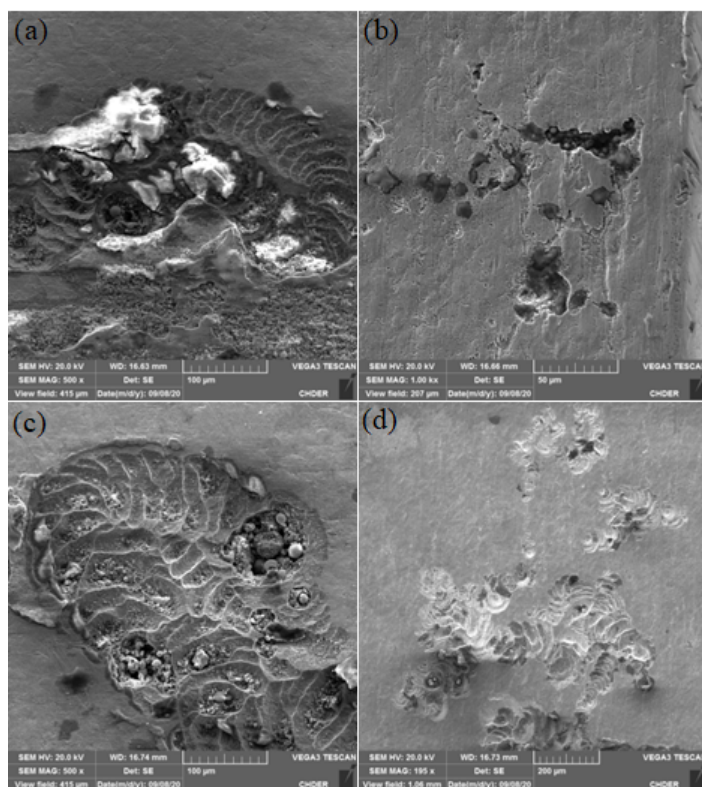

Figure 5. Local corrosion morphology on the inner wall of tube sample: (a) corrosion products of #1 tube; (b) corrosion products of #2 tube; (c) cataphracted corrosion pits of #1 tube;(d) cataphracted corrosion pits of #2 tube.

3.5. EDS Analysis

Energy spectrum analysis experiments were carried out on corrosion pits with cracked inner wall of tube samples. The results are shown in figures 6 and 7, tables 4 and 5. It can be seen that there is no chloride ion in the matrix of #1, #2 tubes, but the chloride ion is detected in the corrosion products near the crack, the content is 0.61% and 0.50%, respectively.
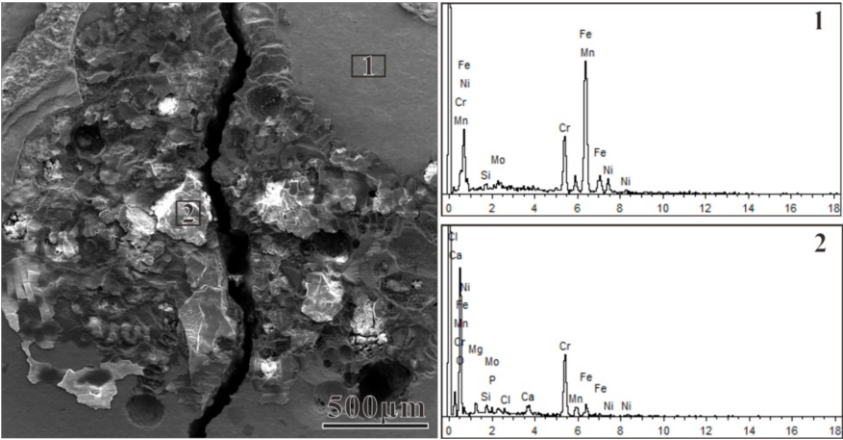
Figure 6. EDS results for #1 sample with two points, 1-matrix, 2-corrosion products.

Table 4. Spectrum results near corrosion pit of #1 sample (Wt. %).

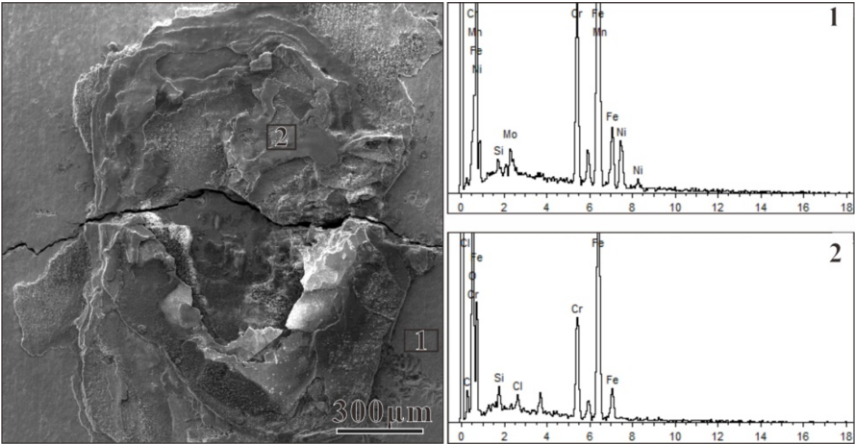| Sites	Si	Cr	Mn	Fe	Ni	Mo	Mg	O	Cl	Ca
point 1	0.57	17.13	0.94	69.36	9.29	2.73	/	/	/	/
point 2	0.98	28.90	0.65	5.18	0.57	3.07	2.36	54.97	0.61	1.52

Figure 7. EDS results for #2 sample with two points, 1-matrix, 2-corrosion products.

Table 5. Spectrum results near corrosion pit of #2 sample (Wt. %).

Sites	Si	Cr	Mn	Fe	Ni	Mo	C	O	Cl
point 1	0.66	16.51	1.32	67.68	10.25	3.58	/	/	/
point 2	0.92	10.35	/	34.22	/	/	7.76	46.26	0.50

4. Discussions

The test results showed that the hardness value, microstructure and tensile properties of the samples all meet the requirements of the relevant standards, but the content of Ni

and Mo in #1 tube is slightly lower than the standard value. The observation of crack morphology demonstrates that the cracks originate at the corrosion pit on the inner wall, and the cracks propagate from the inner wall to the outer wall, along the circumferential direction. In the local area of the inner wall of the tube sample, there are also small corrosion products and cataphracted corrosion pits formed by their shedding from substrate. The connection and confluence of these corrosion pits will lead to the increasing size of corrosion pits and gradually become into the source of cracks. There are dendritic cracks propagating along the outer surface of the tube specimen, which have typical characteristics of stress corrosion crack of stainless steel. The prerequisite of stress corrosion of stainless steel is corrosive medium and tensile stress [8]. According to the theory of phase-forming film, due to its small radius and strong penetrating ability, chloride ions can penetrate the extremely small pores in the oxide film to reach the metal surface, and interact with the metal to form soluble compounds, which will change the structure of the oxide film and cause corrosion of the metal. According to the adsorption theory, chloride ions have a strong ability to be adsorbed by metal, so they are preferentially adsorbed by metal, and the oxygen is discharged from the metal surface. Because oxygen determines the passivation state of the metal, chloride ion and oxygen compete for the adsorption points on the metal surface, and can even replace the passivation ion in the adsorption to form chloride with the metal. The adsorption of chloride and metal surface is not stable, forming a soluble substance. In this way, chloride ion can destroy the oxide film, leading to the acceleration of corrosion.

Outside the heat exchanger tube bundle, the service temperature is 395℃, steam pressure 0.35MPa, while in the tube bundle, service temperature is 70~130℃, water-side pressure is 2.1MPa. The existence of temperature difference will inevitably cause greater thermal stress, while the existence of the tube wall pressure difference will also lead to circumfluential stress. In addition, there may be stress generated by external load, residual stress generated in the process of manufacturing and installation, and several stresses may be coupled into additional tensile stress in the inner wall of the tube.

For the 316L heat exchange tube, critical prerequisite for stress corrosion will be prepared when corrosion medium and tensile stress are introduced during long-term operation. The leakage of two heat exchanger tubes resulted from the cracking of tubes on the inner wall, which generates abundant corrosion products, cataphracted corrosion pits, and severely decreases the performance of heat exchange tube. Therefore, it can be inferred that the cracking of the heat exchanger tube is ascribed to stress corrosion cracking introduced by the lower content of Mo element, excess chloride ions and abnormal stress state in the heat exchanger tubes.

5. Conclusions

(1) The hardness value, microstructure and tensile properties of #1 and #2 tubes meet the requirements of relevant standards, but the contents of Ni and Mo in #1 tubes are slightly lower than the standard requirements, which will decrease the pitting resistance of inner wall of the tubes.

(2) Cracks of the two tube originate from the corrosion pits on the inner wall of the tube, which contained abundant corrosion products with chlorine ions in the pits. The

cracks propagate from the inner wall to the outer wall along the circumferential direction of the tube.

(3) The leakage of the heat exchanger tube can be ascribed to stress corrosion cracking, which is induced by lower content of Mo element, excess chloride ions and abnormal stress state in the heat exchanger tubes.

References

[1]   Fan Q Q 2013 000 *Total. Corr. Contr.* **000** 39.
[2]   Sun S D, Chen W, He S J, Shu Y, Wang X and Wu X Q 2017 *Corr. Prot.* **38** 818.
[3]   Du D H, Shen C, Chen K, Yu L, Zhang L F, Shi X Q and Xu X L 2015 *Chinese J. Eng.* **37** 198.
[4]   Lu H, Du D H, Chen K and Zhang L F 2015 *Atomic Ene Sci Tech* **49** 1849.
[5]   Xia B, Jiang Y and Gong J M 2021 *Hot Work Tech.* **50** 155.
[6]   Wu W B, Zhang Z M, Wang J Q, Han E H and Ke W 2020 *Mater. Rep.* **34** 6144.
[7]   Luo S Z and Peng J G 2007 *Baosteel Tech.* **000** 24.
[8]   Pan X D and Wang X M 2013 *Indus. Water. Treat.* **33** 14.
[9]   Tian H and Liu X H 2021 *Clean World* **37** 19.
[10] Li F Y, Zhang Y M, Xia B J, Dong A H and Shi H W 2007 *Corr. Sci. Prot. Tech.* **19** 304.